Inorganic Chemistry
Cite This: Inorg. Chem. 2019, 58, 9505−9512
Article
pubs.acs.org/IC

Supramolecular Arene-Ruthenium Metallacycle with Thermotropic Liquid-Crystalline Properties

Cristina Alvariño,[†] Benoît Heinrich,[‡] Bertrand Donnio,*[,‡] Robert Deschenaux,[†] and Bruno Therrien*[,†]

[†]Institut de Chimie, Université de Neuchâtel, Avenue de Bellevaux 51, Neuchâtel 2000, Switzerland

[‡]Institut de Physique et Chimie des Matériaux de Strasbourg (IPCMS), UMR 7504, CNRS−Université de Strasbourg, 23 rue du Loess, BP43, Strasbourg cedex 2 67034, France

Supporting Information

ABSTRACT: Functionalization of 1,4-di(4-pyridinyl)-benzene with poly(arylester) dendrimers bearing cyanobiphenyl end-groups gives a bidentate dendromesogenic ligand (**L**) that exhibits thermotropic liquid-crystalline properties. Combination of the diruthenium complex $[Ru_2(p\text{-cymene})_2(donq)][DDS]_2$ (**M**) with **L**, by coordination-driven self-assembly, affords the discrete and well-defined metallacycle $\mathbf{M_2L_2}$. Like **L**, this supramolecular dendritic system displays mesomorphic properties above 50 °C. Both compounds **L** and $\mathbf{M_2L_2}$ show smectic phases, characterized by a multilayered organization of the multiple components.

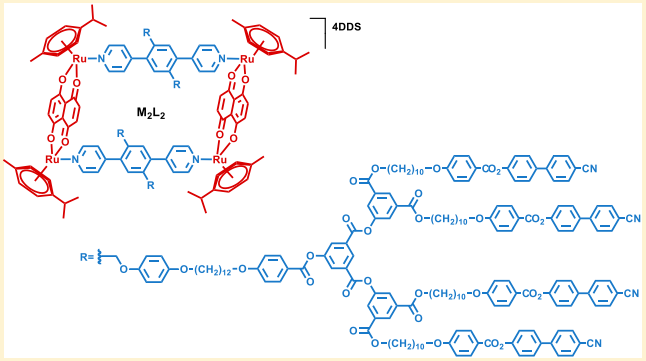

INTRODUCTION

Coordination-driven self-assembly is a successful strategy for the preparation of supramolecular systems from relatively simple starting materials.[1] This strategy is now well-established, and a large variety of discrete two and three-dimensional structures has been produced over the years. Archetypical metallasupramolecular architectures obtained in the last three decades include metallacycles,[2] interlocked molecules,[3] grids,[4] helicates,[5] knots,[6] polyhedra,[7] spheres,[8] metallacages,[9] polymers,[10] and metal−organic frameworks.[11] Self-assembled coordination complexes (SCCs) are not only interesting because of their aesthetical features, they also have potential applications in biology[12] and material sciences.[13] Among SCCs, those incorporating arene ruthenium building blocks have showed great potentials in sensing, drug delivery, and host−guest chemistry.[14]

Hierarchical assembly (HAS) is an attractive method to explore new avenues in soft-matter nanoarchitectures.[15] HAS systems possess a multileveled organization where the first well-defined assembly orders a second organization level via noncovalent interactions, then eventually toward multifunctional structures. Metal−ligand coordination complexes can generate nanoscale HAS, in which the metal complex constitutes the core. Complementary orthogonal interactions such as metal−metal, hydrogen bonding, or $\pi-\pi$ stacking, can be exploited to obtain a second or even a third level of hierarchy in these supramolecular systems.

Liquid-crystalline materials (LCs) have a high importance in nature/life sciences,[16] in modern technologies, displays, optical switching,[17] and recently in biorelated applications, such as chemical and biological sensors[18] or in tissue engineering.[19] The design of functionalized LCs reveals an increasing complexity and they can be composed of covalent connected building-blocks or supramolecular assembled mesogens. Besides, the incorporation of SCCs to LC materials (generally called metallomesogens[20]) offers the possibility of additional intermolecular interactions, such as metal−metal, metal−ligand, and host−guest interactions into stimuli-responsive systems.

LCs are divided in two main families, namely thermotropes and lyotropes. For thermotropic liquid-crystals (TLCs), the mesophases are induced by the temperature, while for lyotropic liquid-crystals (LLCs), the mesophases are controlled by the concentration. Consequently, LCs found in nature are usually lyotropes, because they need to be dispersed in biological media.

Pioneering studies combining SCCs and LCs have been presented by Praefcke and co-workers in the early 1990s.[21] Various series of disk-shaped cyclometalated compounds (Figure 1a) built from palladium and platinum metal centers were synthesized. These large assemblies displayed both thermotropic and lyotropic columnar liquid-crystalline behaviors. Later on, platinum-pyridyl type metallacycle has been prepared by MacLachlan et al. via a head-to-tail association (Figure 1b).[22] They observed a supramolecular aggregation of

Received: May 24, 2019
Published: June 21, 2019

DOI: 10.1021/acs.inorgchem.9b01532
Inorg. Chem. 2019, 58, 9505−9512

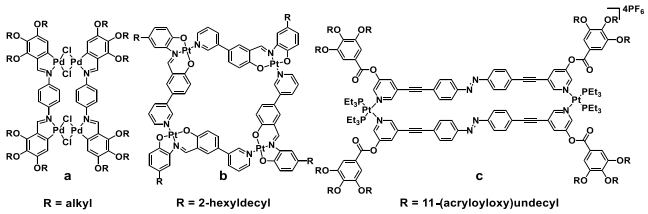

Figure 1. Schematic representation of (a) Praefcke's representative metallacycle, (b) MacLachlan's metallacycle, and (c) Gin's metallacyclic salt.

individual Pt-metallacycle into columnar arrays, thus providing LLC properties to the system. Similarly, the LC behavior of interlocked metallacages has been studied.[23] Septuplet columnar stack of large aromatic molecules with solubilizing side-chain were synthesized via a one-step multicomponent self-assembly process. In aqueous media, the macromolecular septuplet induces LLC phases. More recently, the combination of coordination self-assemblies and dynamic noncovalent interactions has allowed the formation of a giant spherical liquid-crystalline metal-based system.[24] This HAS, containing 24 mesogenic forklike dendrons, exhibits LLC behavior in dimethylformamide.

Only a few examples of TLCs based on a SCC-HAS strategy have been reported so far. Gin and co-workers[25] prepared a dinuclear-Pt mesogenic metallacycle (Figure 1c). This salt possesses a thermotropic columnar hexagonal (Col_H) LC phase that can be swollen by polar solvents to generate a LLC phase. Other elegant examples of SCC TLCs include metallaclusters,[26] metallacycles,[27] catenanes,[28] rotaxanes,[29] grids,[30] and spheres.[24] In most of these above-reported cases, mesomorphism is induced by a "dendritic-type" synthetic strategy via SCC-HAS combinations, which clearly proved efficient but still has not been sufficiently explored.

Over the last two decades, our group has studied liquid-crystalline dendrimers based on cyanobiphenyl frameworks.[31] These systems are well-suited for increasing the number of mesogens and, consequently, the area of the mesogenic part. Moreover, the TLC properties can be tuned by modulating the dendritic generation. Despite some synthetic challenges, this strategy has proven to be very efficient for producing a rich variety of LC materials, and particularly liquid-crystalline fullerenes,[31a,b,d,e,j,k,l] gold nanoparticles,[31f,h,i] metallic clusters,[26c,31c] and luminescent materials.[31g] Previously, a dynamic ordered state was introduced to a ruthenium metallacycle via host–guest interaction from pyrenyl-dendromesogen as a guest.[32] This supramolecular dendritic system showed the formation of highly segregated mesophases with a complex mutlilayered structures in which the cationic metallacycle, the counteranion (dodecyl sulfate) and the guest are equally important. In a similar context, Yu, Tong, and Li have studied the host–guest complexation between a porphyrin-based prism and a pyrenyl dendromesogen.[33] In this particular case, a suppression of the liquid-crystalline behavior was observed after the formation of the host–guest system. Mesomorphism suppression could be due to size differences between the prism and the mesogenic part. Therefore, it is important to highlight the necessity of a good match between the liquid-crystalline promoter and the SCC to retain anisotropic properties to supramolecular HAS systems.

Herein, we have designed a LC dendromesogenic metallacyclic complex via coordination-driven self-assembly. The final assembly contains 16 mesogenic cyanobiphenyl units, covalently linked to the bipyridyl ligands. The use of a bidentate bipyridyl connector with two second-generation dendrons ensures the anisotropic property of the arene ruthenium metallacycle. The liquid-crystalline properties and supramolecular organization of the metallacycle and of the dendritic ligand were investigated by polarized optical microscopy (POM), differential scanning calorimetry (DSC) and small-angle X-ray scattering (SAXS). The metallacycle and the ligand showed a multilayered smectic phase organization. This is a rare example in which the combination of coordination-driven self-assembly and dynamic noncovalent bonding has allowed the formation of a liquid-crystalline metallacycle exhibiting thermotropic properties.

RESULTS AND DISCUSSION

Solution Studies. The tetranuclear arene ruthenium complex ($\mathbf{M_2L_2}$) was prepared in CH_2Cl_2 by combining the dinuclear complex $[Ru_2(p\text{-cymene})_2(donq)][DDS]_2$ (**M**, DDS = dodecyl sulfate) and the bipyridyl ligand (**L**) at room temperature for 24 h (Figure 2) (see the Supporting

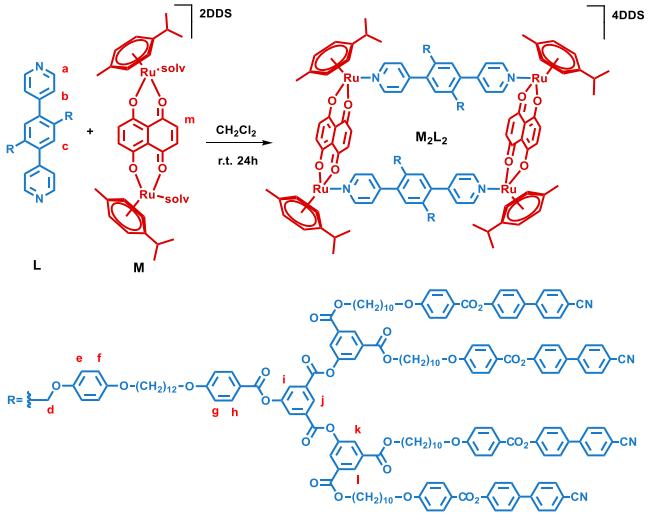

Figure 2. Synthesis of metallacycle $\mathbf{M_2L_2}$ assembled from **M** and dendromesogenic ligand **L**.

Information). The self-assembly of the metallacycle was first confirmed by NMR spectroscopy. The ^1H NMR spectrum shows an upfield shift of the signals of the hydrogen nuclei H_a, H_c, H_d, H_e and H_f upon formation of the metallacycle (Figure 3). The doublet associated with H_a, initially found at δ = 8.62 ppm in the free ligand **L**, is shifted by 0.24 ppm. This shielding is a consequence of the coordination of the pyridyl units to ruthenium ions. On the other hand, the H_b doublet (δ = 7.37 ppm) is almost unaffected by the coordination to the arene ruthenium units. The signals of the protons H_c, H_d, H_e, and H_f are not only shifted to higher frequencies ($\Delta\delta$ = 0.32, 0.30, 0.26, and 0.38 ppm, respectively), they are also affected by a reduction of symmetry due to the loss of rotational freedom of the central phenyl group of the bipyridyl connector **L**. The rotation impediment and the loss of symmetry in $\mathbf{M_2L_2}$ give broad signals for H_c and H_d, and a splitting of the H_e and H_f signals. No shift was observed for the rest of the signals of the ligand as it can be expected.

Diffusion-ordered NMR spectroscopy (DOSY) shows the generation of a large species with a diffusion rate of 0.91 ×

DOI: 10.1021/acs.inorgchem.9b01532
Inorg. Chem. 2019, 58, 9505–9512

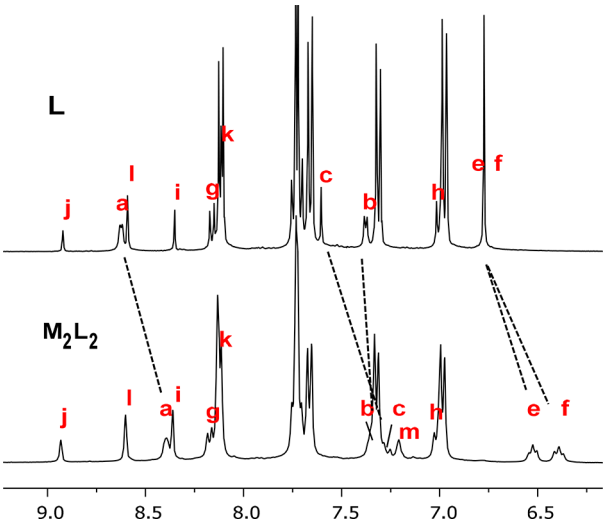

Figure 3. ^{1}H NMR spectra (400 MHz, CD_2Cl_2, 298 K) of ligand **L** (top) and the metallacycle $\mathbf{M_2L_2}$ (bottom).

10^{-10} m^2 s^{-1} (Figure 4). This value is smaller than those of the building blocks **M** and **L**, which possess diffusion coefficients

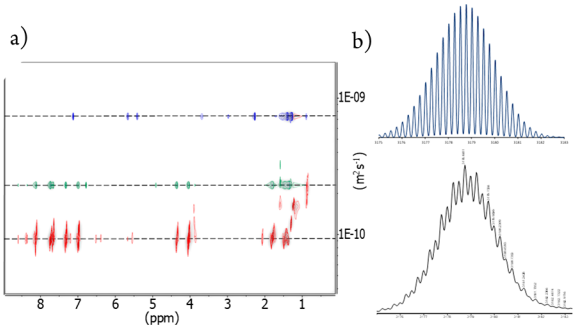

Figure 4. (a) ^{1}H-DOSY spectra (400 MHz, CD_2Cl_2, 298 K) of the compounds **M** (blue), **L** (green), and $\mathbf{M_2L_2}$ (red). (b) Experimental (bottom) and calculated (top) ESI-TOF-MS spectra of $\mathbf{M_2L_2}$ with the loss of four DDS anions: $[\mathbf{M_2L_2} - 4\text{DDS}]^{4+}(m/z = 3178.68)$.

of 7.3. × 10^{-10} m^2 s^{-1} and 2.3 × 10^{-10} m^2 s^{-1}, respectively. From the diffusion coefficient and by using the Stokes–Einstein equation, the diameter of $\mathbf{M_2L_2}$ was estimated to be 106.8 Å. The calculated size matches well with the corresponding lamellar spacing obtained by SAXS measurements (Table S1).

The formation of the metallacycle was further confirmed by electrospray ionization time-of-flight mass spectroscopy (ESI-TOF-MS). As shown in Figure 4, the isotopically resolved peak corresponding to $\mathbf{M_2L_2}$ with the loss of 4 molecules of DDS anions was found at m/z = 3178.68. This peak is in agreement with its calculated theoretical distribution.

Liquid-Crystalline Properties. Both dendritic compounds **L** and $\mathbf{M_2L_2}$ are solids at room temperature in their pristine state. On heating, **L** gave rise to smectic A and nematic phases (Figure 5). The isotropization occurred at 180 °C (Figure S1 and Table S1). The corresponding arene ruthenium metallacycle $\mathbf{M_2L_2}$ is not as thermally stable as **L**, and started to decompose around 160 °C without reaching the isotropic liquid. A birefringent and fluid texture was nevertheless observed by POM just above 50–60 °C, indicating the formation of a thermotropic liquid-crystalline phase (Figure 5).

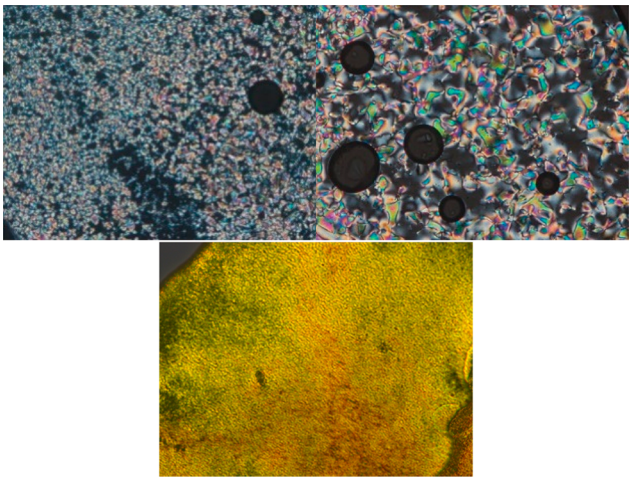

Figure 5. Top: Thermal-polarized optical micrographs of the mesophases displayed by **L**: focal-conic fan texture and homeotropic areas in the SmA-like phase at 166 °C (left), and *Schlieren* texture of the nematic phase at 178 °C (right). Bottom: Thermal-polarized optical micrograph of the mesophase displayed by $\mathbf{M_2L_2}$ at 100 °C.

The structure of the mesophases was investigated by small-angle X-ray scattering (SAXS) between 20 and 100 °C in combination with partial volume calculation. The SAXS patterns confirm that compounds **L** and $\mathbf{M_2L_2}$ self-organize into multilayered smectic-like structures with only short-range correlated lateral arrangements inside the individual layers, as shown by the presence of only wide-angle diffuse scattering signals, aside from the small-angle sharp reflections characterizing the lamellar periodicity (Figures 6 and Figure S2). In

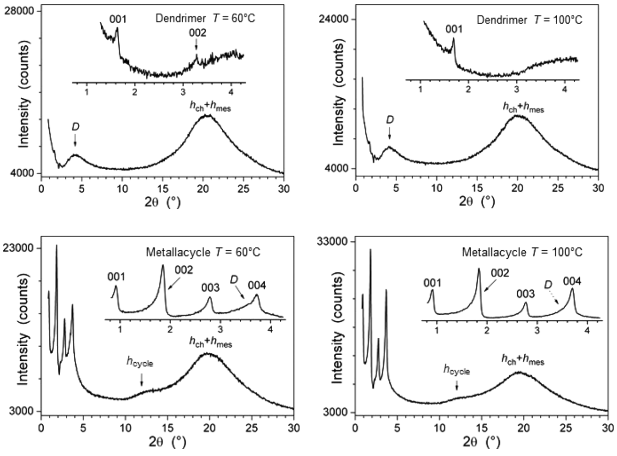

Figure 6. Top: SAXS patterns at 60 and 100 °C with detector (full range) and image plate scans of the small range (inset) for the multilayered smectic A phase formed by **L**. Bottom: SAXS patterns at 60 and 100 °C with detector (full range) and image plate scans of the small range (inset) for multilayered smectic-like lamellar phase formed by $\mathbf{M_2L_2}$.

addition to the usual maximum around 4.5 Å, overlapping the contributions of the terminal cyanobiphenyl mesogens (h_{mes}) and the molten chains (h_{ch}), from the spacers linking the various molecular-blocks and dodecylsulfate segments, all patterns exhibit a scattering signal D in the 20–25 Å range. For **L**, the scattering signal at 21 Å ($\xi \approx 40$ Å) arises from the mean distances between dendritic moieties and phenylene bipyridyl nodes, whereas for $\mathbf{M_2L_2}$, the signal around 25 Å ($\xi \approx$

DOI: 10.1021/acs.inorgchem.9b01532
Inorg. Chem. 2019, 58, 9505–9512

150 Å) is attributed to local range periodicities between metallacycles and dendrimers. The tetranuclear complex $\mathbf{M_2L_2}$

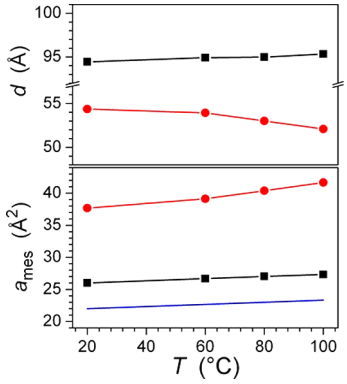

Figure 7. Variation, as a function of the temperature T, of the lamellar periodicity d and of the area per mesogen a_{mes} in the multilayered smectic-like phases formed by **L** (red circles) and $\mathbf{M_2L_2}$ (black squares), $a_{mes} = 2A_{mol}/n_{CB}$ (A_{mol} is the molecular area, and n_{CB}, number of cyanobiphenyl groups per molecule: $n_{CB} = 8$ for **L**, and $n_{CB} = 16$ for $\mathbf{M_2L_2}$); the blue line represents the cross-sectional area of the mesogens, σ_{mes}.

gives rise to a further scattering maximum at 6.5−6.8 Å ($\xi \approx$ 15 Å), attributed to the average spacing of superposed metallacycles (h_{cycle}). The alternation of several high electronic density layers (mesogens, dendritic parts, and nodes/metallacycles) and low-electronic density layers (aliphatic spacers, dodecyl sulfates) explains the strong intensity lowering of the lamellar first-order reflection in all patterns (001 in Figure 6). For the dendrimer, this feature combines with the presence of only one weak higher-order reflection (labeled as 002, Figure 6, top), indicating that the interfaces between successive layers are rather irregular. In contrast, three intense lamellar higher-order reflections (002, 003, 004, Figure 6, bottom) and an attenuated first-order reflection (001, due to the alternation of layers of different electronic densities, as above for **L**) are observed for the metallacycle. In this case, the ionic layers formed by the metallacycles and counterions strongly improve the confinement in the layers and ultimately the sharpness of the interfaces.

It is now assumed that all molecular systems containing polar mesogens as end-groups, such as cyanobiphenyls, self-assemble into smectic phases with the polar mesogens being segregated into either a monolayer or a bilayer structure, i.e., with head-to-tail or head-to-head arrangement of the polar moieties, respectively.[34] Actually, these types of smectic organizations adopt intermediate situations between these two limit cases since both modes of self-associations are in competion. The exact nature of the arrangements and the degree of bilayering, τ, can be easily determined by the molecular areas per end-on mesogen, a_{mes}, whose values range between once (bilayer) or twice (monolayer) the natural cross-section of the mesogen, σ_{mes} (Table S2).[31j,l] The molecular area, A_{mol}, is indeed experimentally accessed by the ratio between the molecular volume, V_{mol}, and the layer periodicity, d, and immediately converted into a_{mes}. The relevant parameter for these systems, the degree of bilayering τ, is then simply quantified by the areas ratio function, defined according to the equation $\tau = 2 - (a_{mes}/\sigma_{mes})$,[31j,l] and leads to a wide-range of τ-values within the smectic phases, varying between zero for monolayers ($\tau = 0$, $a_{mes} = 2\sigma_{mes}$) and one for bilayers ($\tau = 1$, $a_{mes} = \sigma_{mes}$) (Table S2). Here, the layer spacing increases

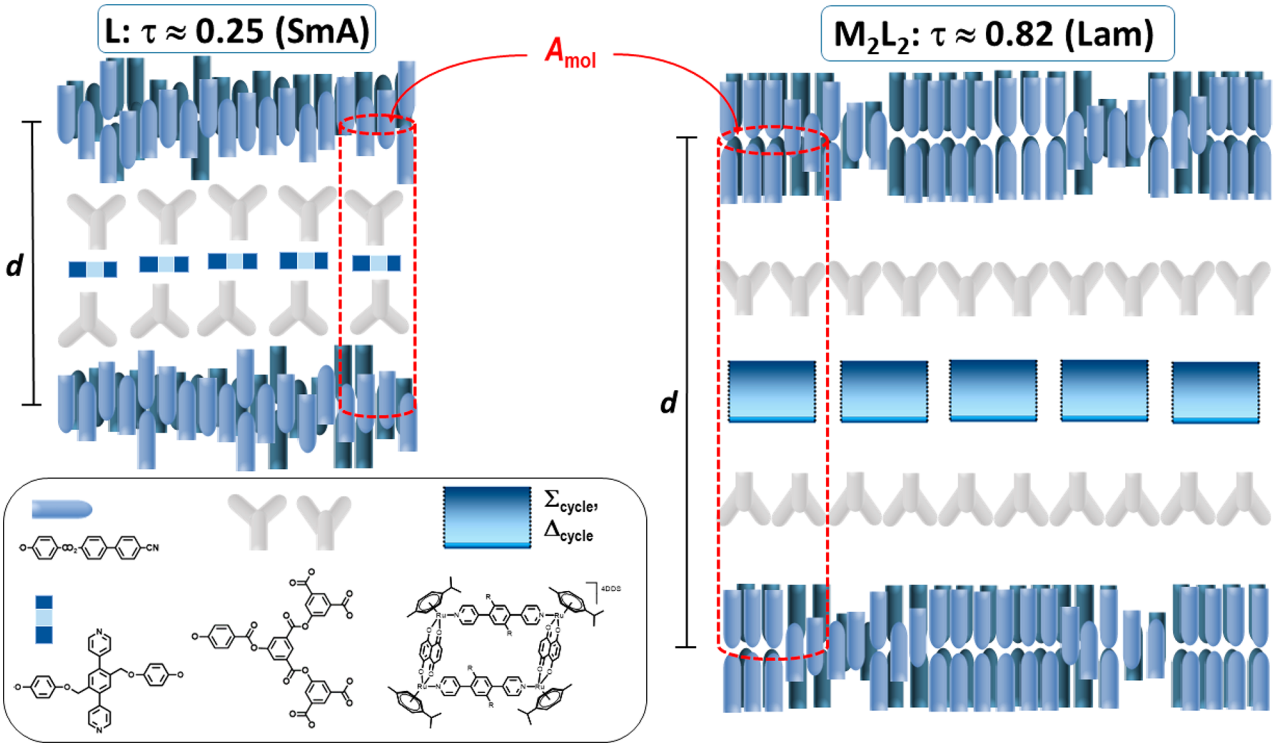

Figure 8. Schematic views of the supramolecular organizations in the multilayered smectic A phase of **L** (left) and in the smectic-like lamellar phase of $\mathbf{M_2L_2}$ (right). d is the lamellar spacing, A_{mol} is the molecular area and $\tau = 2\text{-}(a_{mes}/\sigma_{mes})$ is the bilayering ratio of the mesogen layers.[31j,l] The molten chains (spacers and DDS anions) continuum between the layers is not shown for clarity.

DOI: 10.1021/acs.inorgchem.9b01532
Inorg. Chem. 2019, 58, 9505−9512

drastically by 75% from **L** to $\mathbf{M_2L_2}$ (Figure 7), fully consistent with the substantial decrease of the molecular area per mesogen (a_{mes}) from 38 to 42 Å^2 (**L**) down to 26−27 Å^2 ($\mathbf{M_2L_2}$) (Table S2). Such a large variation reflects the ability of the cyanobiphenyl-terminated mesogens to easily adapt to the molecular areas imposed by the other molecular segments, through the modification of their layer configuration.[3Ij,l]

The further embedded sublayers of the lamellar sequence of the dendrimer are constituted by loosely self-associated segments which may easily vary their degree of lateral spreading through tilting/folding mechanisms, so that the experimental bilayering ratio ($\tau \approx 0.25$) corresponds to the molecular area compromising the optimal average configurations of the individual layers (Figure 8, Table S2).

The low molecular area ($A_{mol} \approx 210$ Å^2) and the high bilayering ratio ($\tau \approx 0.82$) found for the metallacycle presumably emerge from the arrangement of the cycles and counterions into cohesive ionic layers (Table S2, Figure 8). A detailed analysis presupposes knowing the internal structure of these layers, which is not experimentally accessible. To obtain a better understanding of the main features of the lamellar sequence, a rough evaluation of the space requirement of the ions is however sufficient and can be accessed from single crystal structures of model metallacycles devoid of substituents. The molecular organization of such a metallacycle, with the same cyclic architecture as the dendritic complex and close dimensions, is described in the CSD-EGARAG structure.[35] Specifically, the flat-lying cycles and counterions arrange in molecular layers, according to a single-molecule rectangular sublattice (Figure S3). The sublattice area therefore coincides with the cross-sectional area of a molecule in the plane of the cycle, $\Sigma_{cycle} = 285$ Å^2 and the average spacing of metallacycles in parallel to long sides is found to be $\Delta_{cycle} \approx 20$ Å. After taking into account the metallacycle size differences, the dimensions of the ionic layer portion containing a single cycle and counters-ions are estimated to $\Sigma_{cycle} \approx 325$ Å^2 and $\Delta_{cycle} \approx 22$ Å for our compound. The cross sectional area in the cycle side plane ($\sigma_{cycle} \approx \Delta_{cycle} \times h_{cycle} \approx 140-150$ Å^2) is significantly below A_{mol}, which could be compensated by a slight 10−15° tilting of the ionic slabs, as schematically represented in Figure 8. It should, however, be emphasized that this tilting is introduced for the consistency of the analysis and is not accessible otherwise. Ultimately, this approach definitively confirms that the lateral shrinking of lamellae and the switchover from mostly a monolayer to mostly a bilayer configuration of the mesogens is a consequence of the compact and enhanced arrangement within the ionic layers.

CONCLUSIONS

In summary, we have achieved the self-assembly of a novel tetranuclear arene ruthenium metallacycle with a dendritic exofunctionalization. The two poly(arylester) dendritic branches carrying cyanobiphenyl mesogens connected to 1,4-di(4-pyridinyl)benzene are used as liquid-crystalline promoters. Both, ligand and dodecyl sulfate metallacycle, show mesomorphism and they both self-assemble into multilayered smectic phases, whose emergence is promoted by the terminal mesogenic substituents. The tendency of the different molecular components to segregate into different strata of the lamellar periodicity is crucial for the generation of a rare example of SCC-HAS system with thermotropic liquid-crystalline properties. These results pave the way to new applications in the field of coordination-driven self-assembly and hierarchical assembled systems.

ASSOCIATED CONTENT

Supporting Information

The Supporting Information is available free of charge on the ACS Publications website at DOI: 10.1021/acs.inorgchem.9b01532.

Synthesis and characterization of all new compounds (PDF)

AUTHOR INFORMATION

Corresponding Authors

*Email: bruno.therrien@unine.ch.

*Email: bertrand.donnio@ipcms.unistra.fr.

ORCID

Benoît Heinrich: 0000-0001-6795-2733

Bertrand Donnio: 0000-0001-5907-7705

Robert Deschenaux: 0000-0002-1142-0022

Bruno Therrien: 0000-0002-0388-2745

Notes

The authors declare no competing financial interest.

ACKNOWLEDGMENTS

C.A., R.D., and B.T. thank the Swiss National Science Foundation (Grant 200021-162361) for financial support. B.D. and B.H. thank the CNRS and the University of Strasbourg.

DEDICATION

Dedicated to Professor Klaus Bernauer on the occasion of his 85th birthday.

REFERENCES

(1) (a) Stang, P. J.; Olenyuk, B. Self-Assembly, Symmetry, and Molecular Architecture: Coordination as the Motif in the Rational Design of Supramolecular Metallacyclic Polygons and Polyhedra. *Acc. Chem. Res.* **1997**, *30*, 502−518. (b) Chakrabarty, R.; Mukherjee, P. S.; Stang, P. J. Supramolecular Coordination: Self-Assembly of Finite Two- and Three-Dimensional Ensembles. *Chem. Rev.* **2011**, *111*, 6810−6918.

(2) (a) Northrop, B. H.; Zheng, Y.-R; Chi, K.-W; Stang, P. J. Self-Organization in Coordination-Driven Self-Assembly. *Acc. Chem. Res.* **2009**, *42*, 1554−1563. (b) Cook, T. R.; Stang, P. J. Recent Developments in the Preparation and Chemistry of Metallacycles and Metallacages via Coordination. *Chem. Rev.* **2015**, *115*, 7001−7045. (c) Wang, W.; Wang, Y.-X; Yang, H.-B. Supramolecular transformations within discrete coordination-driven supramolecular architectures. *Chem. Soc. Rev.* **2016**, *45*, 2656−2693.

(3) (a) Ayme, J.-F; Beves, J. E.; Campbell, C. J.; Leigh, D. A. Template synthesis of molecular knots. *Chem. Soc. Rev.* **2013**, *42*, 1700−1712. (b) Danon, J. J.; Krüger, A.; Leigh, D. A.; Lemonnier, J.-F; Stephens, A. J.; Vitorica-Yrezabal, I. J.; Woltering, S. L. Braiding a molecular knot with eight crossings. *Science* **2017**, *355*, 159−162. (c) Fielden, S. D. P; Leigh, D. A.; Woltering, S. L. Molecular Knots. *Angew. Chem., Int. Ed.* **2017**, *56*, 11166−11194. (d) Danon, J. J.; Leigh, D. A.; Pisano, S.; Valero, A.; Vitorica-Yrezabal, I. J. A Six-Crossing Doubly Interlocked [2]Catenane with Twisted Rings, and a Molecular Granny Knot. *Angew. Chem., Int. Ed.* **2018**, *57*, 13833−13837.

(4) (a) Ruben, M.; Rojo, J.; Romero-Salguero, F. J.; Uppadine, L. H.; Lehn, J.-M. Grid-type metal ion architectures: functional metallosupramolecular arrays. *Angew. Chem., Int. Ed.* **2004**, *43*, 3644−3662. (b) Hardy, J. G. Metallosupramolecular grid complexes:

DOI: 10.1021/acs.inorgchem.9b01532
Inorg. Chem. 2019, 58, 9505−9512

towards nanostructured materials with high-tech applications. *Chem. Soc. Rev.* **2013**, *42*, 7881−7899. (c) Yang, Q.; Tang, J. Heterometallic grids: synthetic strategies and recent advances. *Dalton Trans.* **2019**, *48*, 769−778.

(5) (a) Piguet, C.; Bernardinelli, G.; Hopfgartner, G. Helicates as Versatile Supramolecular Complexes. *Chem. Rev.* **1997**, *97*, 2005−2069. (b) Piguet, C.; Borkovec, M.; Hamacek, J.; Zeckert, K. Strict self-assembly of polymetallic helicates: the concepts behind the semantics. *Coord. Chem. Rev.* **2005**, *249*, 705−726. (c) Miyake, H.; Tsukube, H. Coordination chemistry strategies for dynamic helicates: time-programmable chirality switching with labile and inert metal helicates. *Chem. Soc. Rev.* **2012**, *41*, 6977−6991. (d) Boiocchi, M.; Fabbrizzi, L. Double-stranded dimetallic helicates: assembling-disassembling driven by the CuI/CuII redox change and the principle of homochiral recognition. *Chem. Soc. Rev.* **2014**, *43*, 1835−1847. (e) Albrecht, M. Helicates: Making head-head-tails of it. *Nat. Chem.* **2014**, *6*, 761−762. (f) Yashima, E.; Ousaka, N.; Taura, D.; Shimomura, K.; Ikai, T.; Maeda, K. Supramolecular Helical Systems: Helical Assemblies of Small Molecules, Foldamers, and Polymers with Chiral Amplification and Their Functions. *Chem. Rev.* **2016**, *116*, 13752−13990.

(6) (a) Raehm, L.; Sauvage, J.-P. Molecular Machines and Motors Based on Transition Metal-Containing Catenanes and Rotaxanes. *Struct. Bonding (Berlin, Ger.)* **2001**, *99*, 55−78. (b) Lukin, O.; Vögtle, F. Knotting and Threading of Molecules: Chemistry and Chirality of Molecular Knots and Their Assemblies. *Angew. Chem., Int. Ed.* **2005**, *44*, 1456−1477.

(7) (a) Amijs, C. H. M; van Klink, G. P. M; van Koten, G. Metallasupramolecular architectures, an overview of functional properties and applications. *Dalton Trans* **2006**, 308−327. (b) Saalfrank, R. W.; Maid, H.; Scheurer, A. Supramolecular coordination chemistry: the synergistic effect of serendipity and rational design. *Angew. Chem., Int. Ed.* **2008**, *47*, 8794−8824. (c) Zangrando, E.; Casanova, M.; Alessio, E. Trinuclear Metallacycles: Metallatriangles and Much More. *Chem. Rev.* **2008**, *108*, 4979−5013.

(8) (a) Sun, Q.-F; Iwasa, J.; Ogawa, D.; Ishido, Y.; Sato, S.; Ozeki, T.; Sei, Y.; Yamaguchi, K.; Fujita, M. Self-assembled $M_{24}L_{48}$ polyhedra and their sharp structural switch upon subtle ligand variation. *Science* **2010**, *328*, 1144−1147. (b) Harris, K.; Fujita, D.; Fujita, M. Giant hollow M_nL_{2n} spherical complexes: structure, functionalisation and applications. *Chem. Commun.* **2013**, *49*, 6703−6712. (c) Fujita, D.; Ueda, Y.; Sato, S.; Mizuno, N.; Kumasaka, T.; Fujita, M. Self-assembly of tetravalent Goldberg polyhedra from 144 small components. *Nature* **2016**, *540*, 563−566. (d) Wang, Q.-Q; Gonell, S.; Leenders, S. H. A. M; Düerr, M.; Ivanović-Burmazović, I.; Reek, J. N. H. Self-assembled nanospheres with multiple endohedral binding sites pre-organize catalysts and substrates for highly efficient reactions. *Nat. Chem.* **2016**, *8*, 225−230. (e) Nonappa; Lahtinen, T.; Haataja, J. S.; Tero, T.-R; Häkkinen, H.; Ikkala, O. Template-Free Supracolloidal Self-Assembly of Atomically Precise Gold Nanoclusters: From 2D Colloidal Crystals to Spherical Capsids. *Angew. Chem., Int. Ed.* **2016**, *55*, 16035−16038. (f) Chen, M.; Wang, J.; Liu, D.; Jiang, Z.; Liu, Q.; Wu, T.; Liu, H.; Yu, W.; Yan, J.; Wang, P. Highly Stable Spherical Metallo-Capsule from a Branched Hexapodal Terpyridine and Its Self-Assembled Berry-type Nanostructure. *J. Am. Chem. Soc.* **2018**, *140*, 2555−2561. (g) Omoto, K.; Hosono, N.; Gochomori, M.; Kitagawa, S. Paraffinic metal-organic polyhedrons: solution-processable porous modules exhibiting three-dimensional molecular order. *Chem. Commun.* **2018**, *54*, 7290−7293.

(9) (a) Forgan, R. S.; Sauvage, J.-P; Stoddart, J. F. Chemical Topology: Complex Molecular Knots, Links, and Entanglements. *Chem. Rev.* **2011**, *111*, 5434−5464. (b) Mukherjee, S.; Mukherjee, P. S. Template-free multicomponent coordination-driven self-assembly of Pd(II)/Pt(II) molecular cages. *Chem. Commun.* **2014**, *50*, 2239−2248. (c) Xu, L.; Wang, Y.-X; Yang, H.-B. Recent advances in the construction of fluorescent metallocycles and metallocages *via* coordination-driven self-assembly. *Dalton Trans.* **2015**, *44*, 867−890. (d) Stoddart, J. F. Mechanically Interlocked Molecules (MIMs)-Molecular Shuttles, Switches, and Machines (Nobel Lecture). *Angew. Chem., Int. Ed.* **2017**, *56*, 11094−11125. (e) Yadav, A.; Gupta, A. K.; Steiner, A.; Boomishankar, R. Mapping the Assembly of Metal-Organic Cages into Complex Coordination Networks. *Chem. - Eur. J.* **2017**, *23*, 18296−18302. (f) Chakraborty, S.; Newkome, G. R. Terpyridine-based metallosupramolecular constructs: tailored monomers to precise 2D-motifs and 3D-metallocages. *Chem. Soc. Rev.* **2018**, *47*, 3991−4016. (g) Pullen, S.; Clever, G. H. Mixed-Ligand Metal-Organic Frameworks and Heteroleptic Coordination Cages as Multifunctional Scaffolds—A Comparison. *Acc. Chem. Res.* **2018**, *51*, 3052−3064.

(10) (a) Chang, D.; Han, D.; Yan, W.; Yuan, Z.; Wang, Q.; Zou, L. Multi-mode supermolecular polymerization driven by host-guest interactions. *RSC Adv.* **2018**, *8*, 13722−13727. (b) Wei, P.; Yan, X.; Huang, F. Supramolecular polymers constructed by orthogonal self-assembly based on host-guest and metal-ligand interactions. *Chem. Soc. Rev.* **2015**, *44*, 815−832. (c) Leong, W. L.; Vittal, J. J. One-Dimensional Coordination Polymers: Complexity and Diversity in Structures, Properties, and Applications. *Chem. Rev.* **2011**, *111*, 688−764.

(11) (a) O'Keeffe, M.; Yaghi, O. M. Deconstructing the Crystal Structures of Metal-Organic Frameworks and Related Materials into Their Underlying Nets. *Chem. Rev.* **2012**, *112*, 675−702. (b) Cheetham, A. K.; Férey, G.; Loiseau, T. Open-Framework Inorganic Materials. *Angew. Chem., Int. Ed.* **1999**, *38*, 3268−3292.

(12) (a) Cook, T. R.; Vajpayee, V.; Lee, M. H.; Stang, P. J.; Chi, K.-W. Biomedical and Biochemical Applications of Self-Assembled Metallacycles and Metallacages. *Acc. Chem. Res.* **2013**, *46*, 2464−2474. (b) Peng, H.-Q; Niu, L.-Y; Chen, Y.-Z; Wu, L.-Z; Tung, C.-H; Yang, Q.-Z. Biological Applications of Supramolecular Assemblies Designed for Excitation Energy Transfer. *Chem. Rev.* **2015**, *115*, 7502−7542.

(13) (a) Lehn, J.-M. Perspectives in Chemistry—Steps towards Complex Matter. *Angew. Chem., Int. Ed.* **2013**, *52*, 2836−2850. (b) Lehn, J.-M. Perspectives in Chemistry—Aspects of Adaptive Chemistry and Materials. *Angew. Chem., Int. Ed.* **2015**, *54*, 3276−3289.

(14) (a) Rauchfuss, T. B., Severin, K. In *Organic Nanostructures*; Atwood, J. L., Steed, J. W., Eds.; Wiley−VCH: New York, 2008; pp 179−203. (b) Singh, A. K.; Pandey, D. S.; Xu, Q.; Braunstein, P. Recent advances in supramolecular and biological aspects of arene ruthenium(II) complexes. *Coord. Chem. Rev.* **2014**, *270*−*271*, 31−56. (c) Therrien, B. The Role of the Second Coordination Sphere in the Biological Activity of Arene Ruthenium Metalla-Assemblies. *Front. Chem.* **2018**, *6*, 602.

(15) (a) Datta, S.; Saha, M. L.; Stang, J. P. HierarchicalAssemblies of Supramolecular CoordinationComplexes. *Acc. Chem. Res.* **2018**, *51*, 2047−2063. (b) Chen, L.-J; Yang, H.-B. Construction of Stimuli-Responsive Functional Materials via Hierarchical Self-Assembly Involving Coordination Interactions. *Acc. Chem. Res.* **2018**, *51*, 2699−2710.

(16) (a) Goodby, J. W. Liquid crystals and life. *Liq. Cryst.* **1998**, *24*, 25−38. (b) Stewart, G. T. Liquid crystals in biology I. Historical, biological and medical aspects. *Liq. Cryst.* **2003**, *30*, 541−557. (c) Stewart, G. T. Liquid crystals in biology II. Origins and processes of life. *Liq. Cryst.* **2004**, *31*, 443−471. (d) Mitov, M. Cholesteric liquid crystals in living matter. *Soft Matter* **2017**, *13*, 4176−4209.

(17) (a) Bos, P. J.; Koehler-Beran, K. R. The pi-Cell: A Fast Liquid-Crystal Optical-Switching Device. *Mol. Cryst. Liq. Cryst.* **1984**, *113*, 329−339. (b) Janicki, S. Z.; Schuster, G. B. A Liquid Crystal Opto-optical Switch: Nondestructive Information Retrieval Based on a Photochromic Fulgide as Trigger. *J. Am. Chem. Soc.* **1995**, *117*, 8524−8527. (c) Wang, L.; Dong, H.; Li, Y. N.; Xue, C. M.; Sun, L.-D; Yan, C.-H; Li, Q. Reversible Near-Infrared Light Directed Reflection in a Self-Organized Helical Superstructure Loaded with Upconversion Nanoparticles. *J. Am. Chem. Soc.* **2014**, *136*, 4480−4483. (d) Wang, J.; Shi, Y.; Yang, K.; Wei, J.; Guo, J. Stabilization and optical switching of liquid crystal blue phase doped with azobenzene-based bent-shaped hydrogen-bonded assemblies. *RSC Adv.* **2015**, *5*, 67357−67364. (e) Jau, H.-C; Li, Y.; Li, C.-C; Chen, C.-W; Wang, C.-T; Bisoyi, H. K.; Lin, T.-H; Bunning, T. J.; Li, Q. Light-Driven Wide-Range

DOI: 10.1021/acs.inorgchem.9b01532
Inorg. Chem. 2019, 58, 9505−9512

Nonmechanical Beam Steering and Spectrum Scanning Based on a Self-Organized Liquid Crystal Grating Enabled by a Chiral Molecular Switch. *Adv. Opt. Mater.* **2015**, *3*, 166−170. (f) Bukusoglu, E.; Bedolla Pantoja, M.; Mushenheim, P. C.; Wang, X.; Abbott, N. L. Design of Responsive and Active (Soft) Materials Using Liquid Crystals. *Annu. Rev. Chem. Biomol. Eng.* **2016**, *7*, 163−196.

(18) Carlton, R. J.; Hunter, J. T.; Miller, D. S.; Abbasi, R.; Mushenheim, P. C.; Tan, L. N.; Abbott, N. L. Chemical and biological sensing using liquid crystals. *Liq. Cryst. Rev.* **2013**, *1*, 29−51.

(19) (a) Woltman, S. J.; Jay, G. D.; Crawford, G. P. Liquid-crystal materials find a new order in biomedical applications. *Nat. Mater.* **2007**, *6*, 929−938. (b) Bera, T.; Freeman, E. J.; McDonough, J. A.; Clements, R. J.; Aladlaan, A.; Miller, D. W.; Malcuit, C.; Hegmann, T.; Hegmann, E. Liquid Crystal Elastomer Microspheres as Three-Dimensional Cell Scaffolds Supporting the Attachment and Proliferation of Myoblasts. *ACS Appl. Mater. Interfaces* **2015**, *7*, 14528−14535. (c) Worthington, K. S.; Green, B. J.; Rethwisch, M.; Wiley, L. A.; Tucker, B. A.; Guymon, C. A.; Salem, A. K. Neuronal Differentiation of Induced Pluripotent Stem Cells on Surfactant Templated Chitosan Hydrogels. *Biomacromolecules* **2016**, *17*, 1684−1695. (d) Martella, D.; Paoli, P.; Pioner, J. M.; Sacconi, L.; Coppini, R.; Santini, L.; Lulli, M.; Cerbai, E.; Wiersma, D. S.; Poggesi, C.; Ferrantini, C.; Parmeggiani, C. Tissue Engineering: Liquid Crystalline Networks toward Regenerative Medicine and Tissue Repair. *Small* **2017**, *13*, 1702677−1702677. (e) Hirst, L. S.; Charras, G. Liquid crystals in living tissue. *Nature* **2017**, *544*, 164−165. (f) Prévôt, M. E.; Andro, H.; Alexander, S. L. M; Ustunel, S.; Zhu, C.; Nikolov, Z.; Rafferty, S. T.; Brannum, M. T.; Kinsel, B.; Korley, L. T. J; Freeman, E. J.; McDonough, J. A.; Clements, R. J.; Hegmann, E. Liquid crystal elastomer foams with elastic properties specifically engineered as biodegradable brain tissue scaffolds. *Soft Matter* **2018**, *14*, 354−360.

(20) (a) Donnio, B.; Guillon, D.; Bruce, D. W.; Deschenaux, R. *Comprehensive Coordination Chemistry II: From Biology to Nanotechnology*; McCleverty, J. A.; Meyer, T. J., Eds.; Elsevier: Oxford, U.K., 2003; Vol. 7, pp 357−627. (b) Pucci, D.; Donnio, B. Metal-containing liquid crystals. In *Handbook of Liquid Crystals*. Goodby, J. W., Collings, P. J., Kato, T., Tschierske, C., Gleeson, H., Raynes, P., Eds.; Wiley−VCH:Weinheim, Germany, 2014; Vol. 5.

(21) (a) Usol'tseva, N.; Praefcke, K.; Singer, D.; Gündogan, B. Lyotropic phase behaviour of disc-shaped tetra-palladium organyls in apolar organic solvents. *Liq. Cryst.* **1994**, *16*, 601−616. (b) Usol'tseva, N.; Praefcke, K.; Singer, D.; Gündogan, B. The first case of a lyotropic twisted nematic (N-) phase induced by a chiral charge transfer complex. *Liq. Cryst.* **1994**, *16*, 617−623. (c) Praefcke, K.; Dielde, S.; Pickardt, J.; Gündogan, B.; Nütz, U.; Singer, D. On the molecular and mesophase structures of disc-like tetrapalladium liquid crystals. *Liq. Cryst.* **1995**, *18*, 857−865. (d) Usol'tseva, N.; Hauck, G.; Koswing, H. D.; Praefcke, K.; Heinrich, B. On the nematic-nematic phase transition in mixtures composed of sheet-shaped palladium organyls and apolar organic solvents. *Liq. Cryst.* **1996**, *20*, 731−739. (e) Praefcke, K.; Holbrey, J. D.; Usol'tseva, N.; Blunk, D. AmphotropicProperties of Multi-Palladium and -PlatinumLiquidCrystals. *Mol. Cryst. Liq. Cryst. Sci. Technol., Sect. A* **1997**, *292*, 123−139. (f) Heinrich, B.; Praefcke, K.; Guillon, D. J. Structural study of columnar liquid-crystalline phases in homologous series of tetrapalladium organyls. *J. Mater. Chem.* **1997**, *7*, 1363−1372. (g) Donnio, B.; Bruce, D. W. Liquid crystalline ortho-palladated complexes. In *Palladacycles - Synthesis, Characterization and Applications*; Pfeffer, M.; Dupont, J., Eds. Wiley-VCH; 2008; pp 239−283.

(22) Frischmann, P. D.; Guieu, S.; Tabeshi, R.; MacLachlan, M. J. Columnar Organization of Head-to-Tail Self-Assembled Pt_4 Rings. *J. Am. Chem. Soc.* **2010**, *132*, 7668−7675.

(23) Yamauchi, Y.; Hanaoka, Y.; Yoshizawa, M.; Akita, M.; Ichikawa, T.; Yoshio, M.; Kato, T.; Fujita, M. m × n Stacks of Discrete Aromatic Stacks in Solution. *J. Am. Chem. Soc.* **2010**, *132*, 9555−9557.

(24) Uchida, J.; Yoshio, M.; Sato, S.; Yokoyama, H.; Fujita, M.; Kato, T. Self-Assembly of Giant Spherical Liquid-Crystalline Complexes and Formation of Nanostructured Dynamic Gels that Exhibit Self-Healing Properties. *Angew. Chem., Int. Ed.* **2017**, *56*, 14085−14089.

(25) Pecinovsky, C. S.; Hatakeyama, E. S.; Gin, D. L. Polymerizable Photochromic Macrocyclic Metallomesogens: Design of Supramolecular Polymers with Responsive Nanopores. *Adv. Mater.* **2008**, *20*, 174−178.

(26) (a) Terazzi, E.; Bourgogne, C.; Welter, R.; Gallani, J.-L; Guillon, D.; Rogez, G.; Donnio, B. Single-Molecule Magnets with Mesomorphic Lamellar Ordering. *Angew. Chem., Int. Ed.* **2008**, *47*, 490−495. (b) Molard, Y.; Dorson, F.; Cîrcu, V.; Roisnel, T.; Artzner, F.; Cordier, S. Clustomesogens: Liquid Crystal Materials Containing Transition-Metal Clusters. *Angew. Chem., Int. Ed.* **2010**, *49*, 3351−3355. (c) Terazzi, E.; Jensen, T. B.; Donnio, B.; Buchwalder, K.; Bourgogne, C.; Rogez, G.; Heinrich, B.; Gallani, J. L.; Piguet, C. Control of the transition temperatures of metallomesogens by specific interface design: application to Mn_{12} single molecule magnets. *Dalton Trans* **2011**, *40*, 12028−12032. (d) Terazzi, E.; Rogez, G.; Gallani, J.-L; Donnio, B. Supramolecular Organization and Magnetic Properties of Mesogen-Hybridized Mixed-Valent Manganese Single Molecule Magnets $[Mn^{III}{}_8Mn^{I}V_4O_{12}(L_{x,y,z\text{-}CB})_{16}(H_2O)_4]$. *J. Am. Chem. Soc.* **2013**, *135*, 2708−2722. (e) Li, W.; Wu, L. Liquid crystals from star-like clusto-supramolecular macromolecules. *Polym. Int.* **2014**, *63*, 1750−1764. (f) Nayak, S. K.; Amela-Cortes, M.; Roiland, C.; Cordier, S.; Molard, Y. From metallic cluster-based ceramics to nematic hybrid liquid crystals: a double supramolecular approach. *Chem. Commun.* **2015**, *51*, 3774−3777. (g) Watfa, N.; Floquet, S.; Terazzi, E.; Haouas, M.; Salomon, W.; Korenev, V. S.; Taulelle, F.; Guénée, L.; Hijazi, A.; Naoufal, D.; Piguet, C.; Cadot, E. Synthesis, characterization, and tuning of the liquid crystal properties of ionic materials based on the cyclic polyoxothiometalate $[\{Mo_4O_4S_4(H_2O)_3(OH)_2\}_2(P_8W_{48}O_{184})]_{36}^{-}$. *Soft Matter* **2015**, *11*, 1087−1099. (h) Molard, Y. Clustomesogens: Liquid Crystalline Hybrid Nanomaterials Containing Functional Metal Nanoclusters. *Acc. Chem. Res.* **2016**, *49*, 1514−1523. (i) Huitorel, B.; Benito, Q.; Fargues, A.; Garcia, A.; Gacoin, T.; Boilot, J.-P; Perruchas, S.; Camerel, F. Mechanochromic Luminescence and Liquid Crystallinity of Molecular Copper Clusters. *Chem. Mater.* **2016**, *28*, 8190−8200.

(27) (a) Barberá, J.; Elduque, A.; Giménez, R.; Lahoz, F. J.; López, J. A.; Oro, L. A.; Serrano, J. L. (Pyrazolato)gold Complexes Showing Room-Temperature Columnar Mesophases. Synthesis, Properties, and Structural Characterization. *Inorg. Chem.* **1998**, *37*, 2960−2967. (b) Kishimura, A.; Yamashita, T.; Yamaguchi, K.; Aida, T. Rewritable phosphorescent paper by the control of competing kinetic and thermodynamic self-assembling events. *Nat. Mater.* **2005**, *4*, 546−549. (c) Kawano, S.; Ishida, Y.; Tanaka, K. Columnar Liquid-Crystalline Metallomacrocycles. *J. Am. Chem. Soc.* **2015**, *137*, 2295−2302. (d) Kawano, S.; Hamazaki, T.; Suzuki, A.; Kurahashi, K.; Tanaka, K. Metal-Ion-Induced Switch of Liquid-Crystalline Orientation of Metallomacrocycles. *Chem. - Eur. J.* **2016**, *22*, 15674−15683.

(28) Baranoff, E. D.; Voignier, J.; Yasuda, T.; Heitz, V.; Sauvage, J.-P; Kato, T. A. Liquid-Crystalline [2]Catenane and Its Copper(I) Complex. *Angew. Chem., Int. Ed.* **2007**, *46*, 4680−4683.

(29) (a) Aprahamian, I.; Yasuda, T.; Ikeda, T.; Saha, S.; Dichtel, W. R.; Isoda, K.; Kato, T.; Stoddart, J. F. A Liquid-Crystalline Bistable [2]Rotaxane. *Angew. Chem., Int. Ed.* **2007**, *46*, 4675−4679. (b) Yasuda, T.; Tanabe, K.; Tsuji, T.; Coti, K. K.; Aprahamian, I.; Stoddart, J. F.; Kato, T. A redox-switchable [2]rotaxane in a liquid-crystalline state. *Chem. Commun.* **2010**, *46*, 1224−1226.

(30) Seredyuk, M.; Gaspar, A. B.; Ksenofontov, V.; Galyametdinov, Y.; Verdaguer, M.; Villain, F.; Gütlich, P. Spin-Crossover and Liquid Crystal Properties in 2D Cyanide-Bridged Fe^{II}-$M^{I/II}$ Metalorganic Frameworks. *Inorg. Chem.* **2010**, *49*, 10022−10031.

(31) (a) Dardel, B.; Guillon, D.; Heinrich, B.; Deschenaux, R. Fullerene-containing liquid-crystalline dendrimers. *J. Mater. Chem.* **2001**, *11*, 2814−2831. (b) Lenoble, J.; Campidelli, S.; Maringa, N.; Donnio, B.; Guillon, D.; Yevlampieva, N.; Deschenaux, R. Liquid-Crystalline Janus-Type Fullerodendrimers Displaying Tunable Smectic-Columnar Mesomorphism. *J. Am. Chem. Soc.* **2007**, *129*, 9941−9952. (c) Frein, S.; Auzias, M.; Sondenecker, A.; Vieille-Petit,

DOI: 10.1021/acs.inorgchem.9b01532
Inorg. Chem. 2019, 58, 9505−9512

L.; Guintchin, B.; Maringa, N.; Süss-Fink, G.; Barberá, J.; Deschenaux, R. MesomorphicMetallo-Dendrimers Based on the Metal-Metal Bonded $Ru_2(CO)_4$ Sawhorse Unit. *Chem. Mater.* **2008**, *20*, 1340−1343. (d) Campidelli, S.; Bourgun, P.; Guintchin, B.; Furrer, J.; Stoeckli-Evans, H.; Saez, I. M.; Goodby, J. W.; Deschenaux, R. Diastereoisomerically Pure Fulleropyrrolidines as Chiral Platforms for the Design of Optically Active Liquid Crystals. *J. Am. Chem. Soc.* **2010**, *132*, 3574−3581. (e) Lincker, F.; Bourgun, P.; Stoeckli-Evans, H.; Saez, I. M.; Goodby, J. W.; Deschenaux, R. Optically active liquid-crystalline fullerodendrimers from enantiomerically pure fulleropyrrolidines. *Chem. Commun.* **2010**, *46*, 7522−7524. (f) Mischler, S.; Guerra, S.; Deschenaux, R. Design of liquid-crystalline gold nanoparticles by click chemistry. *Chem. Commun.* **2012**, *48*, 2183−2185. (g) Mula, S.; Frein, S.; Russo, V.; Ulrich, G.; Ziessel, R.; Barberá, J.; Deschenaux, R. Red and Blue Liquid-Crystalline Borondipyrromethene Dendrimers. *Chem. Mater.* **2015**, *27*, 2332−2342. (h) Nguyen, T. T.; Albert, S.; Nguyen, T. L. A; Deschenaux, R. Liquid-crystalline fullerene-gold nanoparticles. *RSC Adv.* **2015**, *5*, 27224−27228. (i) Nguyen, T. T.; Nguyen, T. L. A; Deschenaux, R. Designing liquid-crystalline gold nanoparticles via the olefin cross-metathesis reaction. *J. Porphyrins Phthalocyanines* **2016**, *20*, 1060−1064. (j) Russo, V.; Pieper, P.; Heinrich, B.; Donnio, B.; Deschenaux, R. Design, Synthesis, and Self-Assembly Behavior of Liquid-Crystalline Bis-[60]Fullerodendrimers. *Chem. - Eur. J.* **2016**, *22*, 17366−17376. (k) Iehl, J.; Nguyen, T. L. A; Frein, S.; Hahn, U.; Barberá, J.; Nienrengarten, J.-F; Deschenaux, R. Designing liquid-crystalline dendronised hexa-adducts of [60]fullerene via click chemistry. *Liq. Cryst.* **2017**, *44*, 1852−1860. (l) Pieper, P.; Russo, V.; Heinrich, B.; Donnio, B.; Deschenaux, R. Liquid-Crystalline Tris[60]fullerodendrimers. *J. Org. Chem.* **2018**, *83*, 3208−3219.

(32) Pitto-Barry, A.; Barry, N. P. E; Russo, V.; Heinrich, B.; Donnio, B.; Therrien, B.; Deschenaux, R. Designing Supramolecular Liquid-Crystalline Hybrids from Pyrenyl-Containing Dendrimers and Arene Ruthenium Metallacycles. *J. Am. Chem. Soc.* **2014**, *136*, 17616−17625.

(33) Yu, G.; Ye, Y.; Tong, Z.; Yang, J.; Li, Z.; Hua, B.; Shao, L.; Li, S. A Porphyrin-Based Discrete Tetragonal Prismatic Cage: Host-Guest Complexation and Its Application in Tuning Liquid-Crystalline Behavior. *Macromol. Rapid Commun.* **2016**, *37*, 1540−1547.

(34) (a) Cardinaels, T.; Driesen, K.; Parac-Vogt, T. N.; Heinrich, B.; Bourgogne, C.; Guillon, D.; Donnio, B.; Binnemans, K. Design of High Coordination Number Metallomesogens by Decoupling of the Complex-Forming and Mesogenic Groups: Nematic and Lamello-Columnar Mesophases. *Chem. Mater.* **2005**, *17*, 6589−6598. (b) Jensen, T. B.; Terazzi, E.; Buchwalder, K. L.; Guénée, L.; Nozary, H.; Schenk, K.; Heinrich, B.; Donnio, B.; Guillon, D.; Piguet, C. Dimerization of Dendrimeric Lanthanide Complexes: Thermodynamic, Thermal, and Liquid-Crystalline Properties. *Inorg. Chem.* **2010**, *49*, 8601−8619. (c) Terazzi, E.; Zaïm, A.; Bocquet, B.; Varin, J.; Guénée, L.; Dutronc, T.; Lemonnier, J.-F; Floquet, S.; Cadot, E.; Heinrich, B.; Donnio, B.; Piguet, C. Implementing Liquid-Crystalline Properties in Single-Stranded Dinuclear Lanthanide Helicate. *Eur. J. Inorg. Chem.* **2013**, *19*, 3323−3333.

(35) Han, Y.-F; Jia, W.-G; Lin, Y.-J; Jin, G.-X. Stepwise Formation of Molecular Rectangles of Half-Sandwich Rhodium and Ruthenium Complexes Containing Bridging Chloranilate Ligands. *Organometallics* **2008**, *27*, 5002−5008.

DOI: 10.1021/acs.inorgchem.9b01532
Inorg. Chem. 2019, 58, 9505−9512